PHYSICAL REVIEW B VOLUME 8, NUMBER 4 15 AUGUST 1973

Electronic Band Structure and Optical Properties of PbTe, PbSe, and PbS†

S. E. Kohn, P. Y. Yu,* Y. Petroff,‡ Y. R. Shen, Y. Tsang, and M. L. Cohen
Department of Physics, University of California
and Inorganic Materials Research Division, Lawrence Berkeley Laboratory, Berkeley, California 94720
(Received 5 September 1972)

By using the techniques of wavelength-modulation spectroscopy, we have measured the reflectivity $R(\omega)$ and the derivative of the reflectivity, $(1/R)dR/d\omega$, for PbTe, PbSe, and PbS from 1.5 to 6 eV. We have independently calculated the band structure, frequency-dependent dielectric function, density of states, and derivative reflectivity spectrum for all three compounds by the empirical pseudopotential method.

I. INTRODUCTION

The narrow-gap IV-VI semiconductors have been the object of extensive research over the past few years.[1-6] Compounds of Pb, Sn, and Ge have been studied, and a great deal is known about many of them. Particular emphasis has been placed on studies of the band-edge properties and the fundamental gap. The location of the gap in the Brillouin zone,[4,5] the temperature and pressure dependence,[6,7] and the alloy dependence of the fundamental gap[7] have been studied extensively. Higher-energy gaps have also been explored, but less is known about these gaps, and few experimental measurements have been made at higher energies.

In this paper we will present experimental optical data and theoretical band-structure calculations for the lead chalcogenides PbTe, PbSe, and PbS. Several band-structure calculations of these compounds are available in the literature using the augmented-plane-wave (APW) method,[8-10] the Korringa-Kohn-Rostoker (KKR) method,[11] the orthogonalized-plane-wave (OPW) method,[12] and two versions of the pseudopotential method.[4,13] All of these calculations have a minimum direct gap at the L point in the Brillouin zone and many other features in common. There are differences, however, of the order of 1 eV for the energy bands away from the fundamental gap. These differences lead to different interpretations of the optical spectrum. These interpretations can be tested by calculating the optical constants in the visible and ultraviolet regions from the various band-structure calculations, and then comparing the results with the measured optical spectra. Some calculations of this kind exist for the IV-VI semiconductors,[5,14,15] but not all of the above band-structure calculations have been tested in this way.

Until recently, the only optical data in the visible and ultraviolet spectral regions available for comparison to theoretical calculations have been the near-normal incidence reflectivity measurements of Cardona and Greenaway,[16] and of Belle.[17] Since these experiments were performed, derivative spectroscopic techniques have become very popular. Aspnes and Cardona[18] have measured the electroreflectance of all three lead salts. In their experiment, the electric field inside the samples was considerably distorted from the ideal square-wave shape because of the high dielectric constant of the compounds. This made the usual interpretation of the electroreflectance data more difficult.[18] Nishino *et al.*[19] have measured the electroreflectance and thermoreflectance of PbSe, showing some differences between these measurements. We have measured the wavelength-modulated reflectance of PbTe, PbSe, and PbS from 1.5 to 6 eV at temperatures ranging from 5 to 300 °K. The only previously published wavelength-modulation reflectivity measurements on any of these compounds is the work of Korn, Welkowsky, and Braunstein on the $Pb_xSn_{1-x}Te$ alloy system.[20]

We have also made empirical-pseudopotential-method (EPM) calculations of the band structure and $\epsilon_2(\omega)$ spectrum of PbSe and PbS. In addition, by Kramers-Kronig transformations of the theoretical $\epsilon_2(\omega)$ spectrum, the reflectivity derivative spectrum $(1/R)dR/d\omega$ is calculated for PbTe, PbSe, and PbS, and compared with the experimental measurements. These results confirm the critical-point assignment for the $\epsilon_2(\omega)$ spectrum of PbTe made previously by Cohen and Tsang.[7] By using the method of Gilat and Dolling,[21] we have also calculated the density of states for all three compounds.

II. EXPERIMENTAL PROCEDURE

The theory of wavelength-modulation spectroscopy and a description of our experimental apparatus has been given elsewhere.[22] A double-beam optical system is used to normalize the reflectivity and to cancel the background contributions to the derivative signal. The system is operated in a configuration that measures $R(\lambda)$ and $dR/Rd\lambda$ simultaneously. These results are then converted to $R(\omega)$ and $dR/Rd\omega$ by a relatively simple com-

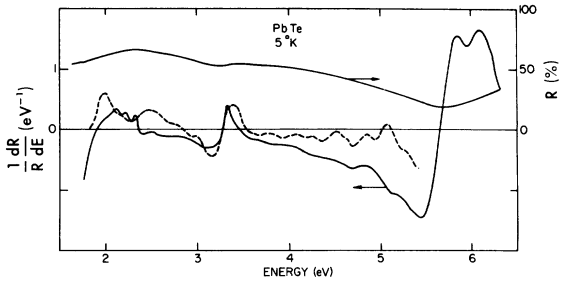

FIG. 1. Reflectivity and derivative reflectivity of PbTe at 5 °K. The dotted curve is the theoretical $(1/R)dR/d\omega$ spectra calculated by EPM.

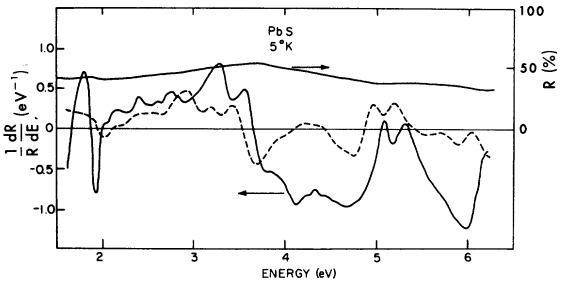

FIG. 3. Reflectivity and derivative reflectivity of PbS at 5 °K. The dotted curve is the theoretical $(1/R)dR/d\omega$ spectra calculated by EPM.

puter manipulation.

Samples of all three compounds studied were bulk single crystals. All of the samples used were cleaved to produce a clean flat surface and immediately placed in the optical Dewar. The PbS crystal was large and cleaved very well. The crystals of PbTe and PbSe were relatively small, and their cleavages were not as perfect. Therefore, the absolute magnitude of their reflectivity measurements may not be correct, though the relative measurements are still very acceptable. Once inside the Dewar, the samples were continuously maintained in a helium atmosphere. Temperature control was achieved by flowing helium gas past the samples. The spectra thus obtained are always reproducible, indicating that surface contamination has no observable effect on our spectra.

We have also investigated the effect of surface electric field on the structures in our spectra by measuring two PbS samples with carrier concentrations ~ 10^{16} and ~ 10^{18} cm^{-3}, respectively. We have found no difference between the spectra of these two samples except the structure at 5.08 eV, which has a stronger temperature dependence than the other structures as we will show in Sec. V. Thus we are led to conclude that, except for this 5.08-eV structure, our derivative spectrum of PbS is not affected by the surface field. The same thing is probably true for the other two lead salts although we did not have the crystals to perform the same measurements as in PbS. The same conclusion would be obtained if one estimates the effect of surface field on the wavelength-modulated spectra of the lead salts using an expression recently obtained by Seraphin and Aspnes.[23]

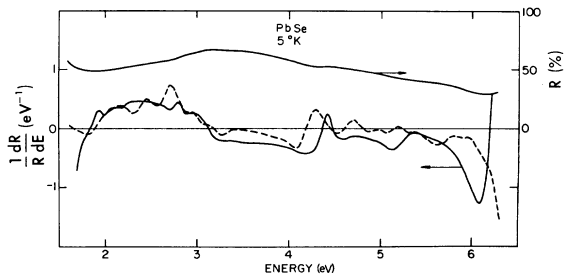

FIG. 2. Reflectivity and derivative reflectivity of PbSe at 5 °K. The dotted curve is the theoretical $(1/R)dR/d\omega$ spectra calculated by EPM.

III. EXPERIMENTAL RESULTS

The experimentally measured reflectivity spectra $R(\omega)$, and derivative reflectivity spectra $dR/Rd\omega$ for PbTe, PbSe, and PbS are presented in Figs. 1–3 along with theoretical calculations of the derivative spectra. All experimental results presented here were measured at 5 °K. The main feature of the $dR/Rd\omega$ spectrum of PbTe agrees quite well with the results of Korn *et al.*[20] at 80 °K. The derivative spectrum of all three compounds are strikingly similar. In all of the spectra, the E_2 and E_3 structures (in the notation of Cardona and Greenaway[16]) are well resolved. It is of particular interest to note the fine structure in the derivative spectra, particularly the existence of several peaks on the low-energy side of the E_2 peak. These peaks are very similar in the spectra of all three compounds.

A Kramers-Kronig analysis of the $dR/Rd\omega$ spectra was performed to determine $\epsilon_1(\omega)$, $\epsilon_2(\omega)$, $d\epsilon_1/d\omega$, and $d\epsilon_2/d\omega$. The results of these calculations are presented in Figs. 4 and 5. A description of the method of calculation is given in the Appendix. The results agree well with those of Korn *et al.*[20] in the case of PbTe. A quick glance at the $\epsilon_2(\omega)$ and $d\epsilon_2/d\omega$ spectra shows that the $d\epsilon_2/d\omega$ spectra reveals considerably more structure than the $\epsilon_2(\omega)$ spectra, and is therefore useful in identifying critical points and finer details of the optical spectrum.

Critical points obtained from the experimental spectra are listed in Table I, along with experimental results of previous work. They were determined in two ways. First, critical points in the reflectivity were determined from the $dR/Rd\omega$ spectra. However, in the Kramers-Kronig analy-

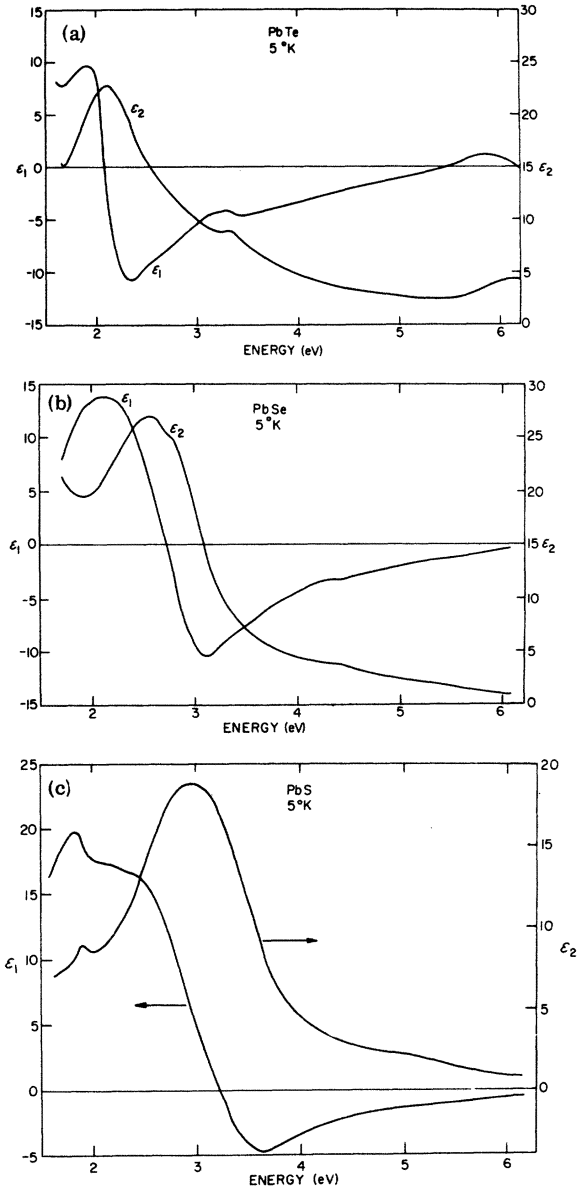

FIG. 4. $\epsilon_1(\omega)$ and $\epsilon_2(\omega)$ of (a) PbTe, (b) PbSe, and (c) PbS calculated by Kramers-Kronig analysis of the $(1/R)dR/d\omega$ spectra.

sis of the experimental data, structures were shifted. Therefore, a second list of critical-point energies determined from the $d\epsilon_2/d\omega$ spectra is given. The identification of these transitions then follows from a comparison with the critical-point energies in the $\epsilon_2(\omega)$ spectra calculated by EPM.

It is possible for structures in $(1/R)dR/d\omega$ to originate from structures in $\epsilon_1(\omega)$ rather than $\epsilon_2(\omega)$. Aspnes and Cardona[18] showed that, in electroreflectance, $\Delta R \propto -\Delta\epsilon_1$ near the E_2 peak for all three lead salts. A close comparison of our experimental data and the calculated $d\epsilon_1/d\omega$ confirms this result.

IV. CALCULATION

The EPM has now been widely applied to many compounds, and the pseudopotential form factors for many elements (extracted from different EPM band-structure calculations) are now available. These existing pseudopotential form factors $V(q)$ for Pb, Se, and S are plotted, respectively, in Figs. 6 and 7.[24] A smooth curve is drawn through each set. The values of the form factors can be read directly from these curves and can be properly scaled to the lattice constants of PbSe and PbS to give the starting set of form factors. The lattice constants of PbSe and PbS are taken to be 6.124 and 5.936 Å. Following the EPM scheme, these form factors are slightly adjusted to fit several optical gaps. The choice of these optical gaps are based on the assumption that the corresponding structures in the reflectivity spectrum in PbS and PbSe arise from the same regions of the Brillouin zone as in PbTe, which have been anal-

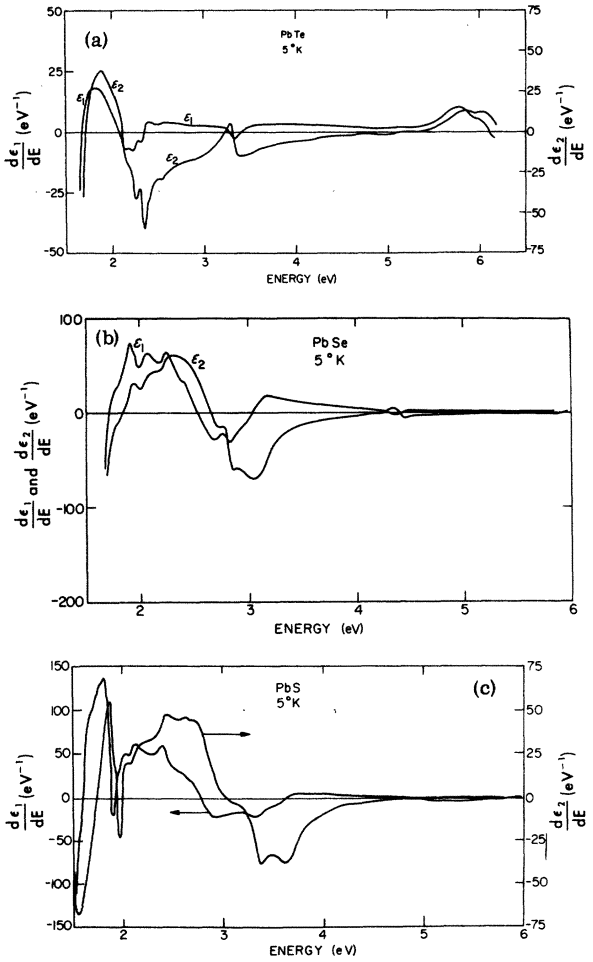

FIG. 5. $d\epsilon_1/d\omega$ and $d\epsilon_2/d\omega$ of (a) PbTe, (b) PbSe, and (c) PbS calculated by Kramers-Kronig analysis of the $(1/R)dR/d\omega$ spectra.

TABLE I. Critical-point energies of (a) PbTe, (b) PbSe, and (c) PbS. The second column contains critical points derived from experimentally measured $(1/R)dR/d\omega$. [(w) stands for weak.] The third column has critical points from the $d\epsilon_2/d\omega$ spectra obtained by Kramers-Kronig analysis. The fourth column contains the results of EPM calculations.

Region	Other experimental data	$\frac{1}{R}\frac{dR}{d\omega}$	$\frac{d\epsilon_2}{d\omega}$	Theory	CP symm.	Transition
		(a) PbTe[a]				
E_0	0.190[e]			0.19	M_0	$L(5\rightarrow6)$
E_1	1.24			1.07	M_1	$\Sigma(5\rightarrow7)$
				1.27	M_0	$L(5\rightarrow7)$
		2.16(w)[d]				
E_2	2.18[c]	2.25[d]	2.1	2.00	M_1	$\Sigma(5\rightarrow7)$
		2.36[d]	2.2	2.03	M_2	$\Delta(5\rightarrow6)$
	2.45[c]	2.56(w)[d]	2.3			
E_3	3.5[b]	3.47	3.3	2.78	M_2	$\Delta(4\rightarrow6)$
		4.83(w)	4.9	3.1	M_1	$\Sigma(4\rightarrow7)$
		5.9	5.9			
E_4	6.3[b]					
					Volume effects	
E_5	7.8[b]				transitions near X	
E_6	11.2[b]					
		(b) PbSe				
E_0	0.165[e]			0.172	M_0	$L(5\rightarrow6)$
E_1	1.59[b]			1.6	M_0	$L(5\rightarrow7)$
	1.54[c]	1.97(w)	2.0	1.9	M_1	$\Sigma(5\rightarrow6)$
	1.78[c]	2.18(w)	2.15	2.3	M_0	$L(4\rightarrow6)$
E_2	2.95[b]	2.84(w)[d]	2.65	2.7	M_1	$\Sigma(5\rightarrow7)$
	3.12[b]	3.12[d]	2.8	2.9	M_2	$\Delta(5\rightarrow6)$
	3.3[c]					
	3.8[c]					
E_3	4.5[b]	4.47	4.40	4.2	M_2	$\Delta(4\rightarrow6)$
	4.6[c]	5.52	5.3	4.3	M_1	$\Sigma(4\rightarrow7)$
E_4	7.1[b]					
					Volume effects	
E_5	9.1[b]				transitions near Γ and X	
E_6	12.5[b]					
		(c) PbS				
E_0	0.286[e]			0.287	M_0	$L(5\rightarrow6)$
E_1	1.85[b,c]	1.9	2.0	1.6	M_0	$L(5\rightarrow7)$
	1.98	2.15	2.1	1.9	M_1	$\Sigma(5\rightarrow6)$
		2.46	2.3			
		2.85	2.5			
E_2	3.49[b]	3.35[d]	3.0			
	3.7[c]	3.66[d]	3.3	2.94	M_1	$\Sigma(5\rightarrow7)$
	4.0[c]	4.01[d]	3.9(w)	3.5	M_2	$\Delta(5\rightarrow6)$
	4.6[c]	4.5[d]				
E_3		5.08	5.0	4.92	M_1	$\Sigma(4\rightarrow7)$
	5.27[b]	5.31	5.2	5.1	M_2	$\Delta(4\rightarrow6)$
		5.75(w)				
E_4	8.1[b]					
					Volume effect	
E_5	9.8[b]				transitions near Γ and X	
E_6	13.9[b]					

[a]Reference 4.
[b]Reference 16.
[c]Reference 18.
[d]Structure in $(1/R)\ dR/d\omega$ due to structure in ϵ_1.
[e]Reference 26.

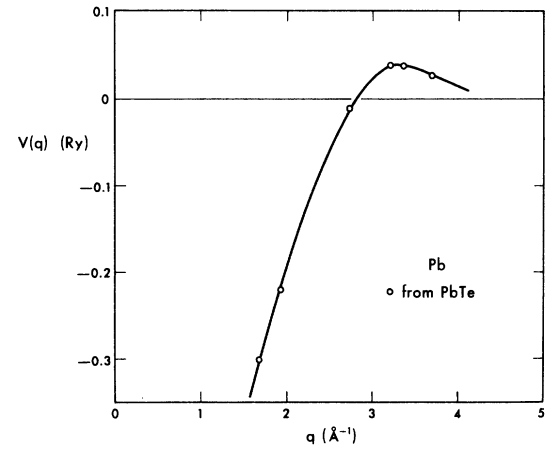

FIG. 6. Pseudopotential form factors for Pb. The points are derived from PbTe data (Refs. 23 and 24).

yzed previously.[4] In Table II are listed the starting set of form factors for PbS and PbSe interpolated and scaled from the Pb, S, and Se potentials,[24] as discussed above. This table also contains the final set used in calculating the band structure and optical properties. The starting and final sets of form factors are remarkably close. The adjustment from the former to the latter set is minimal.

Spin-orbit coupling effects are included in the EPM calculation. The symmetric and antisymmetric spin-orbit parameters λ_S, λ_A[24,25] in each material are chosen so that the ratio λ_S/λ_A corresponds to that of the constituent outermost core atomic spin-orbit splitting.

The resultant band structure for PbSe and PbS

TABLE II. Interpolated and final set of pseudopotential form factors used for the calculation of the band structures of PbSe and PbS.

	PbSe		PbS	
	Interpolated (Ry)	Final adjusted (Ry)	Interpolated (Ry)	Final adjusted (Ry)
$V^S(4)$	−0.2334	−0.2377	−0.256	−0.2532
$V^S(8)$	−0.0171	−0.0171	−0.0116	−0.0181
$V^S(12)$	0.0097	0.0097	0.0242	0.0242
$V^A(3)$	0.0657	0.0735	0.091	0.0859
$V^A(11)$	0.0154	0.01224	0.0154	0.01038

are shown in Figs. 8 and 9, respectively. The minimum direct gap E_g is at the L point of the Brillouin zone with symmetry L_6^+ for the top valence band and symmetry L_6^- for the bottom conduction band, as in PbTe. The fundamental gaps are 0.172 and 0.287 eV, respectively, for PbSe and PbS. From studies of interband magnetoabsorption, the corresponding experimentally measured values are 0.165± 0.005 and 0.286± 0.003 eV.[26] The over-all features of the band structures for PbSe and PbS are similar and resemble that for PbTe (Fig. 10).

An intrinsic property of an EPM calculation is that the high-energy bands crowd together as a result of the truncation of the Hamiltonian matrix.[24] This is illustrated by the PbS conduction bands at Γ. In a nonrelativistic calculation, the conduction-band symmetry at Γ for the lead salts would be Γ_{15}, $\Gamma_{25'}$, and Γ_{12}, counting upward in energy from the forbidden gap. The spin-orbit coupling splits the Γ_{15} into Γ_6^- and Γ_8^-, $\Gamma_{25'}$ to Γ_7^+ and Γ_8^+, and Γ_{12} to Γ_8^+.

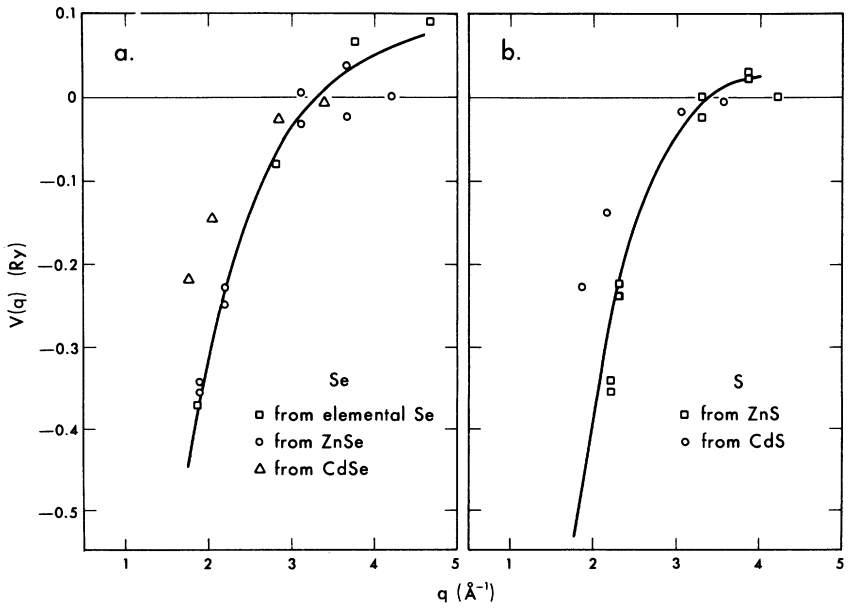

FIG. 7. Pseudopotential form factors for (a) Se and (b) S (Refs. 23 and 24).

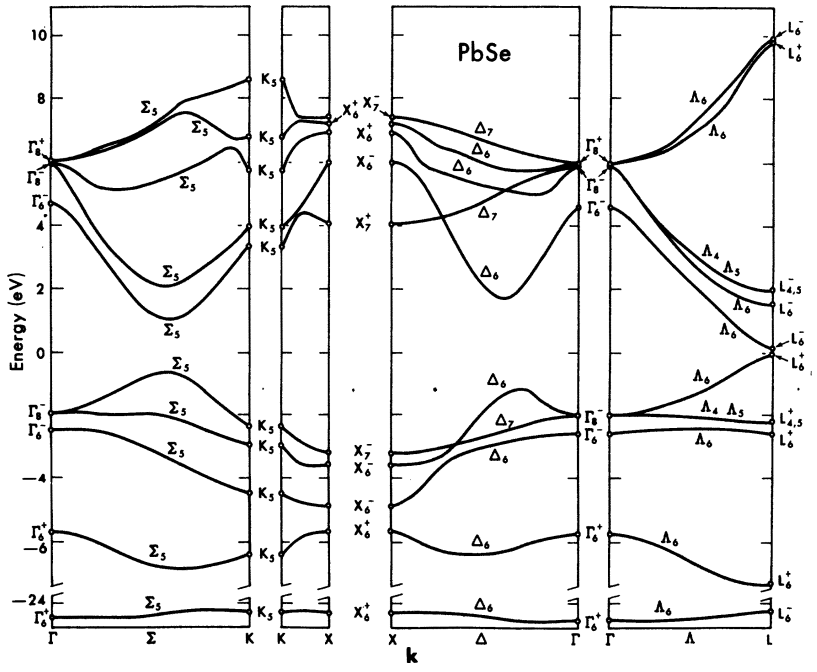

FIG. 8. Energy-band structure of PbSe.

In PbS, the levels arising from $\Gamma_{25'}$ and Γ_{12} crowd together as they decrease in energy away from, and drop below, the Γ_8^- level of Γ_{15}. This same effect of the crowding of the higher-energy bands is seen in the optical spectrum where the energies of the theoretical high-energy structure (E_4, E_5, E_6) deviate somewhat from the measured data.

The imaginary part of the frequency-dependent dielectric function $\epsilon_2(\omega)$ has the form

$$\epsilon_2(\omega)=\frac{e^2\hbar^2}{3\pi m^2\omega^2}\sum_{c,v}\int \delta\,(E_c(\vec{k})-E_v(\vec{k})-\hbar\omega) \times|\langle u_{\vec{k},v}\,|\vec{\nabla}\,|u_{\vec{k},c}\rangle|^2 d^3\vec{k}, \quad (1)$$

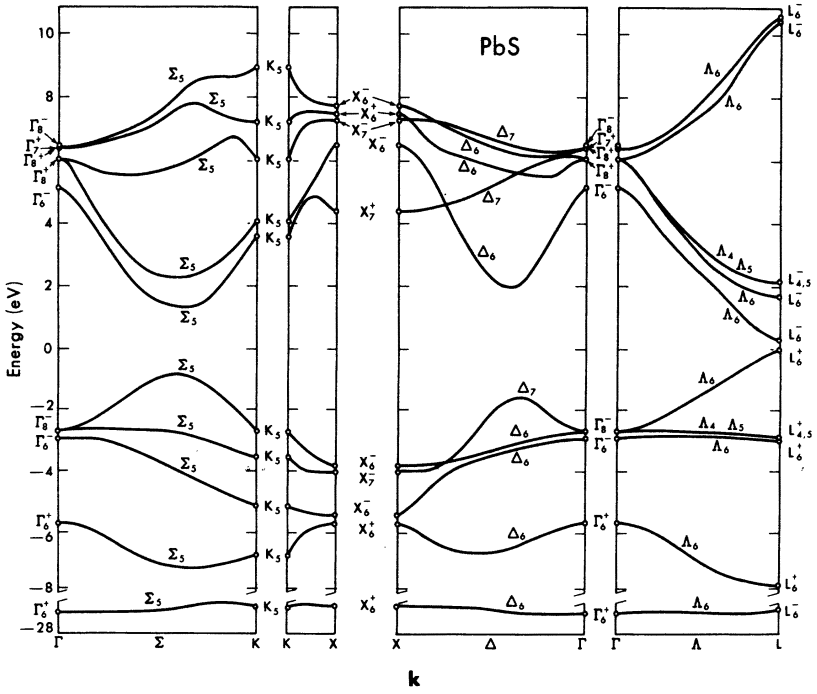

FIG. 9. Energy-band structure of PbS.

where $u_{\vec{k},v}$ and $u_{\vec{k},c}$ are the periodic parts of the valence- and conduction-band Bloch wave functions at $\vec{k}$ and $E_v(\vec{k})$ and $E_c(\vec{k})$ are the energies of these states. In the previous calculation of $\epsilon_2(\omega)$ for PbTe, [4] these wave functions and energies are obtained by diagonalizing a pseudopotential Hamiltonian at 356 mesh points in the irreducible part of the fcc cubic Brillouin zone. Approximately 3×10^6 random sampling points are then chosen using a Monte Carlo method. The energy eigenvalues and dipole matrix elements associated with each point are chosen by linear interpolation between the 356 mesh points. The prominent structure in the $\epsilon_2(\omega)$ originate from Van Hove singularities[24] at critical points where $\nabla_{\vec{k}}[E_c(\vec{k})]=0$. This can be more clearly seen if we write the k integration in Eq. (1) in terms of an integration over a surface S, corresponding to a constant interband energy difference $E_c(\vec{k})-E_v(\vec{k})$. Assuming the dipole matrix to be a constant,

$$\epsilon_2 \sim \int \frac{dS}{|\nabla_{\vec{k}}[E_c(\vec{k})-E_v(\vec{k})]|} . \qquad (2)$$

The expression on the right-hand side in Eq. (2) is the joint density of states.

Gilat and Dolling[21] developed a different method of calculation first applied to a computation of the phonon density of states for a cubic crystal. [27] This method proved to be of much higher resolution, speed, and accuracy in comparison with traditional random-point sampling methods. This method also involves dividing the irreducible section of the first Brillouin zone into a cubic mesh, but instead of taking discrete random points within the mesh, the constant frequency surfaces inside every small cube are approximated by a set of parallel planes [the directions of the planes are determined by $\nabla_{\vec{k}}E(\vec{k})$ at the mesh points] and may be continuously integrated. Since the spectra contain two important factors, the density of states and the transition probability or dipole matrix element, these have to be known accurately when comparing with experimentally measured spectra. Gilat and coworkers obtain such accuracy for the density of states in Refs. 21 and 27 by treating the matrix element of each cube as a constant. This implies that fine details of the computed spectrum could be significantly distorted. The computation of the matrix elements was later taken to the same degree of accuracy as the density of states by Gilat and Kam. [28]

Along with the experimental derivative reflectivity data of the present work, we employ the Gilat scheme[21,27] in computing the $\epsilon_2(\omega)$ for PbTe, PbSe, and PbS. The pseudo-Hamiltonian is diagonalized at 308 $\vec{k}$ points within the irreducible part of the Brillouin zone. The mesh chosen is slightly different from the former calculation for PbTe [4] in that here the mesh points are shifted away from symmetry directions to avoid degeneracy, a necessary condition of the Gilat scheme. For this calculation, the dipole matrix element inside each mesh is taken to be a constant equal to the value at the mesh point. This is done for two reasons. First of all, previous experience with PbTe indicates the usefulness of even the joint density of states in determining the origin of the main structure in the reflectivity. Second, a first-order perturbation calculation on the dipole matrix element at the mesh point to allow interpolation between points requires far more computer time than doing a perturbation calculation on the energy. Therefore, as a first attempt, we have taken the matrix elements as constant in each small cubic mesh.

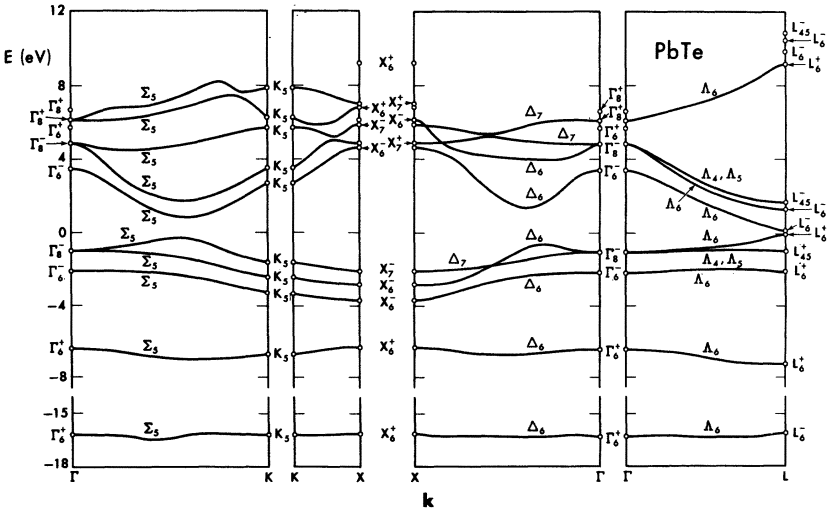

FIG. 10. Energy-band structure of PbTe (a reproduction from Ref. 4).

V. DISCUSSION

The final theoretical results are presented in Figs. 1–3 and the theoretical $dR/Rd\omega$ spectra are shown as dashed lines in Figs. 1–3, together with the experimental spectra. The corresponding band structures for PbSe, PbS, and PbTe are given in Figs. 8–10, respectively. In Fig. 11, the corresponding $\epsilon_2(\omega)$ spectra are shown. They agree well with the $\epsilon_2(\omega)$ (Fig. 4) obtained from the experimental data.

The peaks in $\epsilon_2(\omega)$ are typically shifted down in energy from the reflectivity spectrum by about 0.3 eV. The purpose of the theoretical and experimental $\epsilon_2(\omega)$ curves (Figs. 11 and 4) is then to display the position of the main peaks and shoulders, whereas the experimental and theoretical derivative reflectivity spectra (Figs. 1–3) are designed to display the fine structure on the main ones. In Table I are listed our critical-point assignments for PbTe,[7] PbSe, and PbS using the EPM calculations, and experimental values of critical points obtained by us and by others[16,18] for the E_1-E_6 structures. Note that the critical-point assignments for all three materials are almost identical. The values of E_4, E_5, and E_6 in the theoretical E_2 all group together and are shifted down in energy, owing to the crowding of higher-energy conduction bands previously discussed.

To obtain the theoretical $dR/Rd\omega$ spectra, $\epsilon_1(\omega)$ was calculated from the theoretical $\epsilon_2(\omega)$ by Kramers-Kronig transformation using an appropriate tail function[29] for frequencies above ω_{cutoff}.[24] The respective ω_{cutoff} for PbTe, PbSe, and PbS are 8.5, 9.0, and 9.5 eV.

In the following discussion for the results of the PbTe, PbSe, and PbS, the notations E_0-E_6 of Cardona and Greenaway[16] will be used freely since the optical spectra for the three materials are indeed qualitatively similar and discussion of a qualitative nature is applicable to all three cases.

(i) *PbTe* [*Figs.* 1 *and* 11(a)]. The solid curve in Fig. 11(a) is the previous theoretical $\epsilon_2(\omega)$ calculation obtained from a random-point sampling. The dotted curve is the present calculation using the Gilat sampling scheme. Note how the critical points are accentuated in the present (Gilat) scheme. The approximation that dipole matrix elements are constant within each cube in the present scheme shows up most obviously at the bumps at 0.3, 0.6, and 1.2 eV. The previous random-point sampling scheme, which gives less resolution than the present scheme when structure arises from critical-point singularities, does take account of the interpolation of dipole matrix elements within the cubic mesh. So in case of fine structures arising mainly from volume effects, such as those at 0.3, 0.6, and 1.2 eV in PbTe, the random-point sampling scheme probably portrays the actual $\epsilon_2(\omega)$ better than the Gilat scheme. Otherwise, the agreement for the energy positions and the general profile between the experimental and theoretical $\epsilon_2(\omega)$ using the Gilat scheme is good. The theoreti-

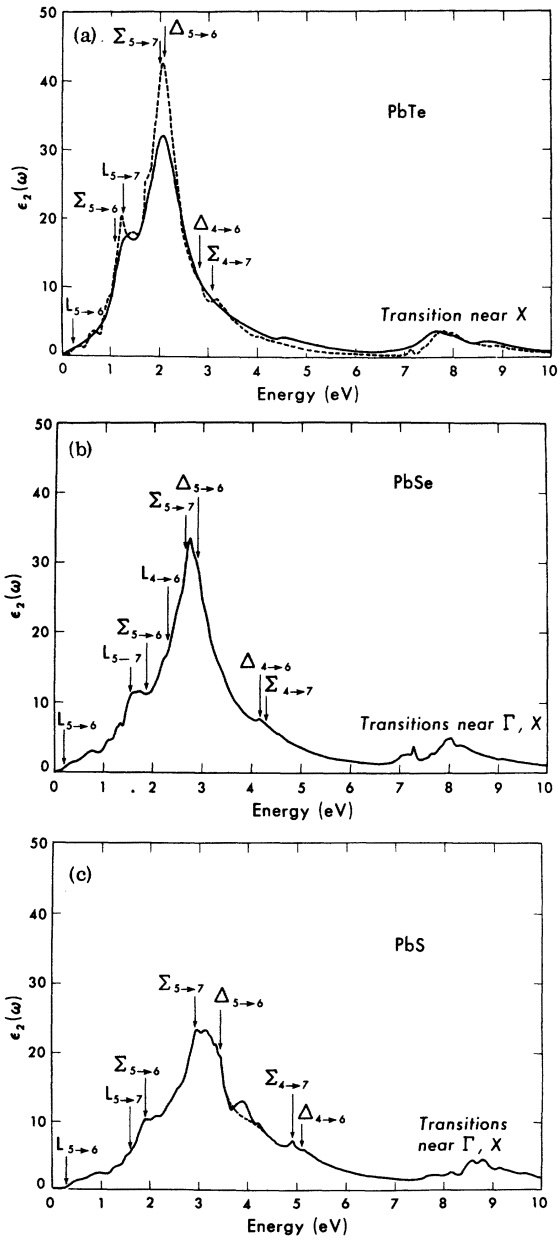

FIG. 11. Theoretical imaginary part of the frequency-dependent dielectric function $\epsilon_2(\omega)$ for (a) PbTe, (b) PbSe, and (c) PbS. In case of PbTe the two theoretical curves correspond to two different sampling schemes: the Gilat scheme (broken curve) and the random-point sampling scheme (solid curve). The 4-eV peak in PbS is artificial and disappears when linear interpolation for the matrix elements is used in this energy range (dotted line). For details, see text.

cal derivative reflectivity spectrum derived from $\epsilon_3(\omega)$ is extremely sensitive to any slight variation of the slope as well as the main peaks and shoulders in the $\epsilon_2(\omega)$. A comparison of the theoretical $(1/R)dR/d\omega$ with experiment in Fig. 1 is therefore encouraging. The theoretical $dR/Rd\omega$ would resemble the experimental curve at 3.35 eV if the E_3 shoulder in the theoretical $\epsilon_2(\omega)$ were slightly flatter. The experimental $dR/Rd\omega$ curve changes slope from negative to positive at 5.4 eV due to an upward turn of slope in $\epsilon_2(\omega)$ at energies just below the E_4(6.3 eV as measured from reflectivity) structure. The theoretical E_4 value is at 7.1 eV, and thus the theoretical $dR/Rd\omega$ continues to have a negative slope at 5.4 eV. These results seem to indicate that our previous critical-point assignments[4] for PbTe were essentially correct.

(ii) *PbSe* [*Figs. 2 and* 11(b)]. One essential feature that differentiates PbSe from PbTe in the experimental $dR/Rd\omega$ spectrum (Fig. 2) is the broad structure with small peaks between 2.0 and 3.1 eV in the $dR/Rd\omega$ spectrum. The corresponding structure in PbTe (Fig. 1) is much narrower, having a width of only 0.5 eV. This can be understood from the theoretical critical-point analysis (Table I) and the theoretical $\epsilon_3(\omega)$ curves [Figs. 11(a) and 11(b)]. For PbSe, there are critical points at 1.9 and 2.3 eV, both with moderate dipole matrix elements. The main peak E_2 is composed of two critical points with large dipole matrix elements at 2.7 and 2.9 eV. This cluster of critical points with increasing dipole matrix elements gives rise to the gentle rising E_2 peak. In PbTe, the critical points with moderate dipole matrix elements occur at 1.07 and 1.27 eV while those with large dipole matrix elements are at 2.00 and 2.02 eV. Thus in PbTe, critical points with moderate matrix elements are more widely separated from those with large matrix elements than in PbSe. Furthermore, the two critical points with large matrix elements in PbTe occur at almost the same energy. These result in a sharper and narrower E_2 peak in PbTe than in the case of PbSe.

The small structure on the main peaks arises from varying dipole matrix elements for different regions of k space. As can be seen by the above arguments, both the position of the critical points and the dipole matrix elements are important to give the optical spectrum. This point will be even more apparent when discussing PbS. The structure near the 4.4-eV region in the experimental $dR/Rd\omega$ (Fig. 2) is again due to the E_3 shoulder in $\epsilon_2(\omega)$ and the rise in slope at 6.1 eV again arises because of the E_4 structure at 7.1 eV.

(iii) *PbS* [*Figs. 3 and* 11(c)]. The theoretical $\epsilon_2(\omega)$ in Fig. 11(c) shows that in addition to the E_1-E_6 structure, there is an extra bump between 3.5 and 4.1 eV. No critical point is found in this energy region. A close examination of all the energy gaps that may contribute to $\epsilon_2(\omega)$ in this energy range uncovers the following: (a) the contribution to this part of $\epsilon_2(\omega)$ arises from the same band transitions in neighboring cubic mesh, i.e., volume effect (each mesh covers an energy level of about 0.2–0.3 eV), and (b) the dipole matrix elements of these neighboring mesh points vary by a factor of 2 or 3. Recall that the matrix element in each cubic mesh is taken to be constant and equal to the value at the mesh point, whereas the energy is allowed to vary continuously within the mesh. Therefore in the continuous energy range of above 6.6 eV, the dipole matrix element jumps discontinuously by about a factor of 2 to 3 at every 0.2 or 0.3 eV interval.

If one now uses linear interpolation for the matrix elements in the continuous energy range of these particular neighboring cubic mesh points in question, the resultant $\epsilon_2(\omega)$ between 3.5 and 4.1 eV will follow the dotted line in Fig. 11(c). In the region of the spurious bump, there remains now only some smooth structure, which does show up when transformed to the theoretical $(1/R)dR/d\omega$ in Fig. 3. This structure deviates considerably in shape from the experiment $(1/R)dR/d\omega$ in the region from 3.5 to 4.5 eV. The Gilat scheme[21] would be necessary if one were interested in obtaining an undistorted spectrum and retaining the qualitative features of the fine structures of the optical spectrum, because it takes into account the interpolation of the matrix elements within each cubic mesh. The distortion of the fine structure is especially important when the structure arises from volume effects. In PbSe and PbTe, the E_3 critical points are close in energy to the E_2 critical points. The singularities help to mask the distortion of fine structures arising from the approximation imposed on the dipole matrix elements. We are less fortunate in PbS in that E_3 critical points are much higher in energy than the E_2 critical points, allowing volume effects to dominate in between. The structure between 2 and 3.5 eV in the experimental $(1/R)dR/d\omega$ (Fig. 3) is even broader than the corresponding one in PbSe. This is again a result of the clustering of critical points at 1.6, 1.9, 2.94, and 3.5 eV. Note the two large matrix element critical points that give rise to the E_2 peak (2.94 and 3.5 eV) are separate by 0.56 eV. This gives rise to a very broad E_2 peak.

In measuring the reflectivity spectrum of PbS as a function of temperature, we observe a pronounced sharpening in the fine structure at 5.08 eV as the temperature decreases. This sharpening is observable even between liquid-nitrogen and liquid-helium temperatures. This is shown in Fig. 12. No other structure in the spectra of all three compounds has a similar behavior. The

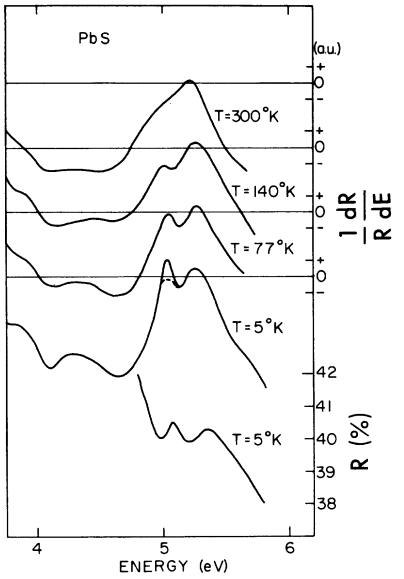

FIG. 12. Temperature dependence of the derivative reflectivity $(1/R)dR/d\omega$ of PbS around the E_3 structure.

sample used in this measurement was n type with a carrier concentration of $\sim 10^{16}/\mathrm{cm}^3$ as obtained from Hall-effect measurements. However, when we repeated the measurement on an n-type sample with a carrier concentration of $\sim 10^{18}/\mathrm{cm}^3$, we obtained exactly the same spectra as the other sample, except this 5.08-eV structure, which became less pronounced at low temperature, and did not show appreciable change as the temperature varied from 80 to 5 °K. This result, similar to what was observed for the E_1 peaks of Ge, [30] indicates that this structure is not simply due to band transitions. The strong temperature dependence together with the dependence on the carrier density seems to suggest that the structure may be due to excitonic effect. According to Table I (c), the E_3 peak is due to M_1 and M_2 critical-point transitions at Σ and Δ, and hence, based on the Toyozawa model, [31] hyperbolic excitons can exist in the E_3 peak. One may use the high dielectric constant of PbS to argue against the idea of excitons in PbS. However, in our case, the excitons involving electrons in the high conduction bands may see a smaller effective dielectric constant than even the high-frequency dielectric constant ϵ_∞. The free carriers tend to screen the attractive interaction between electrons and holes, and this would explain why the excitonic effect decreases with higher carrier concentration in our observation.

For completeness, we also present theoretical calculations of the density of states of PbTe, PbSe, and PbS in Fig. 13. Again, these are based on the EPM band structures and the Gilat sampling scheme. The valence-band edge is taken to be the zero-energy reference. The energy ranges from -12 to $+12$ eV. This energy range covers four valence bands and five conduction bands. The lowest valence band in the EPM calculation for the three materials are more than 13 eV below the top valence-band edge. Since these band structures have given reasonable results in explaining the reflectivity data, one would anticipate that the density of states could also be useful in studying photoemission experiments. [32]

Wavelength-modulation spectroscopy has proved capable of detecting many fine structures in the op-

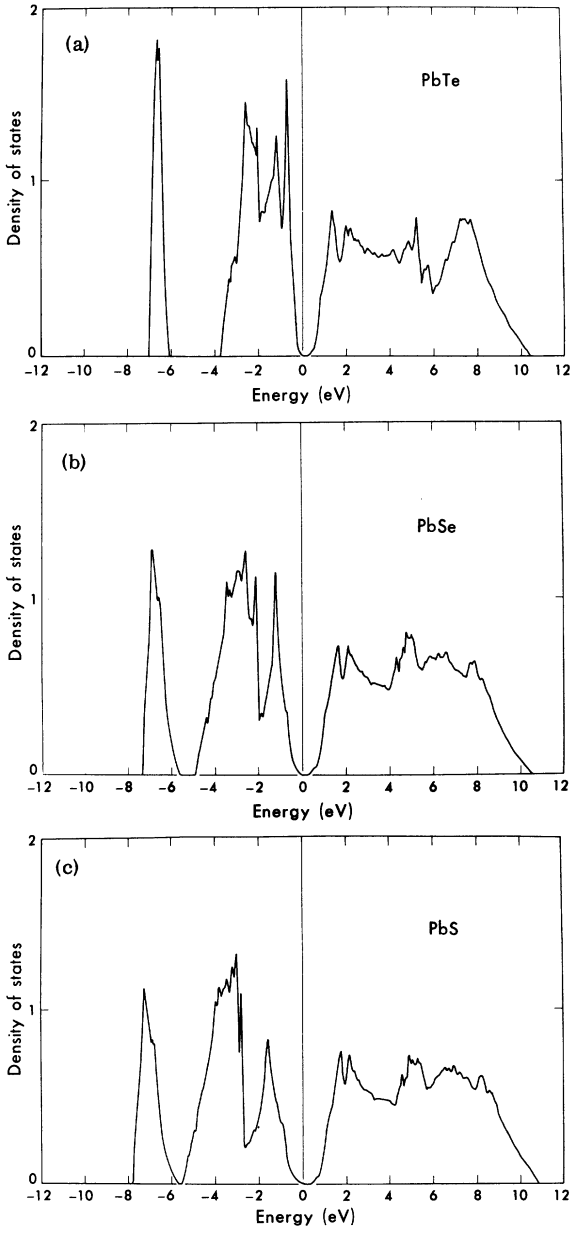

FIG. 13. Density of states (number of states per eV per primitive cell) for (a) PbTe, (b) PbSe, and (c) PbS.

tical spectrum of PbTe, PbSe, and PbS. The agreement of the experimental and theoretical $(1/R)\,dR/d\omega$ and $\epsilon_2(\omega)$ is quite good. Based upon these results, we conclude that the EPM gives band structures of the lead chalcogenides that are essentially correct throughout the Brillouin zone. With these band structures, we have gained confidence in a more thorough understanding of the optical properties of the lead chalcogenides. The computational techniques may be improved by changing the approximation used in handling the dipole matrix elements. If this is done, we believe that the band-structure calculations are capable of giving not only the main structure but also the very fine structure in the optical reflectivity spectra.

ACKNOWLEDGMENTS

One of us (Y. W. Tsang) would like to thank John Joannopoulos for helpful discussions on the Gilat scheme of computation. We would also like to thank M. Mulrey for assistance in preparing some of the graphs.

APPENDIX: KRAMERS-KRONIG ANALYSIS

To obtain $\epsilon_1(\omega)$ and $\epsilon_2(\omega)$, we need to know both the absolute reflectivity $R(\omega)$ and the corresponding phase angle $\theta(\omega)$.[33] These two quantities are related by the Kramers-Kronig relation

$$\theta(\omega) = -\frac{\lambda}{\pi}\int_0^\infty d\lambda' \frac{\ln R(\lambda')}{(\lambda')^2-\lambda^2} \quad . \tag{A1}$$

This can be transformed into the form

$$\theta(\lambda) = -\frac{1}{2\pi}\int_0^\infty d\lambda' \frac{d\ln R}{d\lambda}(\lambda') \ln\left|\frac{\lambda+\lambda'}{\lambda-\lambda'}\right| , \tag{A2}$$

which is more appropriate for our own case, since we measure $d\ln R/d\lambda$ with greater accuracy than R. This method of calculation has the disadvantage that the function $\ln|(\lambda+\lambda')/(\lambda-\lambda')|$ does not go to zero as fast as $1/(\lambda'^2-\lambda^2)$ as λ' becomes very different from λ. Hence, the calculation is a little more sensitive to the extrapolation conditions used for the low- and high-energy limits of the integral.

By differentiating Eq. (A2) with respect to λ, we have

$$\frac{d\theta}{d\lambda}(\lambda) = -\frac{1}{\pi}\int_0^\infty d\lambda' \frac{d\ln R}{d\lambda}(\lambda') \frac{\ln R(\lambda')}{(\lambda')^2-\lambda^2} \quad . \tag{A3}$$

The derivatives of ϵ_1 and ϵ_2 can then be calculated from $d\ln R/d\lambda$ and $d\theta/d\lambda$.

In evaluating the integrals for θ and $d\theta/d\lambda$, it is necessary to make truncating approximations for the low- and high-energy limits of the integrals. It is well known that the reflectivity of semiconductors becomes approximately constant at very low energies. It is common to take $R(\lambda)$ as constant for long wavelengths when computing θ via Eq. (A1).[33] We have made a similar approximation $d\ln R/d\omega = 0$ for long wavelengths. Also, structure in $d\ln R/d\lambda$ far away from the long-wavelength limit of Eqs. (A2) and (A3) tend to oscillate around zero, giving small contributions to the integrals. At very high energies, it is expected, from a Drude type of dielectric function, that the reflectivity should decrease roughly as ω^{-4}. Therefore, we approximated a functional dependence for R of ω^{-A}, where A is an adjustable parameter around 4. To make the calculations less sensitive to A, the room-temperature reflectivity data of Cardona and Greenaway[16] from 6 to 20 eV were used in computing the integrals. The results are very insensitive to the choice of A used. Varying A by over a factor of 2 does not change the shape of the curves appreciably, but does change the over-all magnitudes somewhat. The absolute magnitudes of the curves are also somewhat in error because the absolute magnitude of $(1/R)\,dR/d\lambda$ is a little uncertain, although this does not have a very strong effect in the Kramers-Kronig analysis.

---

†Work supported in part by the U. S. Atomic Energy Commission and the National Science Foundation, Grant No. GP 13632, A1.

*IBM Postdoctoral Fellow.

‡On leave from the University of Paris.

[1] M. L. Cohen, Y. Tung, and P. B. Allen, J. Phys. (Paris) Suppl. **29**, C4-163 (1968).

[2] *The Physics of Semimetals and Narrow Gap Semiconductors: Proceedings of the Conference held at Dallas, Texas, 20–21 March 1970*, edited by D. L. Carter and R. T. Bates (Pergamon, New York, 1971).

[3] Proceedings of the Conference on the Physics of IV-VI Compounds and Alloys, Philadelphia, 1972 (unpublished).

[4] Y. W. Tung and M. L. Cohen, Phys. Rev. **180**, 823 (1969); Phys. Rev. B **2**, 1216 (1970); Y. W. Tung and M. L. Cohen, Phys. Lett. A **29**, 236 (1969).

[5] Y. W. Tsang and M. L. Cohen, Solid State Commun. **9**, 261 (1971).

[6] Y. W. Tsang and M. L. Cohen, Phys. Rev. B 3, 1254 (1971).

[7] M. L. Cohen and Y. W. Tsang, Ref. 2, p. 303.

[8] L. E. Johnson, J. B. Conklin, Jr., and G. W. Pratt, Jr., Phys. Rev. Lett. **11**, 538 (1963); J. B. Conklin, Jr., L. E. Johnson, and G. W. Pratt, Jr., Phys. Rev. **137**, A1282 (1965).

[9] L. G. Ferreira, Phys. Rev. **137**, A1601 (1965).

[10] S. Rabii, Phys. Rev. **167**, 801 (1968); S. Rabii, Phys. Rev. **173**, 918 (1968).

[11] H. Overhof and V. Rössler, Phys. Status Solidi **37**, 691 (1970).

[12] F. Herman, R. L. Kortum, I. Ortenburger, and J. P. Van Dyke, J. Phys. (Paris) Suppl. **29**, C4–62 (1968).

[13] P. J. Lin and L. Kleinman, Phys. Rev. **142**, 478 (1966).

[14] See Ref. 1.

[15] D. D. Buss and N. J. Parada, Phys. Rev. B 1, 2692 (1970).

[16] M. Cardona and D. L. Greenaway, Phys. Rev. **133**, A1685 (1964).

[17]M. L. Belle, Fiz. Tverd. Tela **5**, 3282 (1963) [Sov. Phys.-Solid State **5**, 2401 (1964)]; Fiz. Tverd. Tela **7**, 606 (1965) [Sov. Phys.-Solid State **7**, 480 (1965)].
[18]D. E. Aspnes and M. Cardona, Phys. Rev. **173**, 714 (1968).
[19]T. Nishino, H. Ogawa, and Y. Hamaka, J. Phys. Soc. Jap. **30**, 1113 (1971).
[20]D. M. Korn, M. Welkowsky, and R. Braunstein, Solid State Commun. **9**, 2001 (1971); D. M. Korn and R. Braunstein, Phys. Rev. B 5, 4837 (1972).
[21]G. Gilat and G. Dolling, Phys. Lett. **8**, 304 (1964).
[22]R. R. L. Zucca, Ph.D. thesis (University of California, Berkeley, 1970) (unpublished).
[23]B. O. Seraphin and D. E. Aspnes, Phys. Rev. B 6, 3158 (1972).
[24]M. L. Cohen and V. Heine, in *Solid State Physics*, edited by H. Ehrenreich, F. Seitz, and D. Turnbull (Academic, New York, 1970), Vol. 24. The data points in Figs. 6, 7(a), and 7(b) are taken directly from Tables 15 and 16, pages 212 and 215.
[25]Y. W. Tsang, Ph.D thesis (University of California, Berkely, 1970) (unpublished).
[26]D. L. Mitchell, E. D. Palik, and J. N. Zemel, in *Physics of Semiconductors, Paris, 1964*, edited by M. Hulin (Academic, New York, 1964), p. 325.
[27]G. Gilat and L. J. Rankenheimer, Phys. Rev. **144**, 390 (1966).
[28]G. Gilat and Z. Kam, Phys. Rev. Lett. **22**, 715 (1969).
[29]J. P. Walters and M. L. Cohen, Phys. Rev. **183**, 763 (1969).
[30]Y. Petroff, S. E. Kohn, and Y. R. Shen, in First International Conference on Modulation Spectroscopy, Tucson, Arizona, November, 1972 (unpublished).
[31]Y. Toyozawa, M. Inoue, M. Okazaki, and E. Hanamura, J. Phys. Soc. Jap. Suppl. **21**, 133 (1967).
[32]A very good agreement with the theoretical valence-band density of states has been obtained by photoemission measurements on PbTe: R. Pinchaux, Y. Petroff, D. Dagneaux, and M. Balkanski, in Conference on Physics of IV-VI Compounds and Alloys, Philadelphia, 24–25 March 1972 (unpublished); and W. E. Spicer and G. J. Lapeyre, Phys. Rev. **139**, A565 (1965). After this work has been completed, x-ray photoemission [F. R. McFeely, S. Kowalczyk, L. Ley, R. A. Pollak, and D. A. Shirley, Phys. Rev. B (to be published)] and uv photoemission [M. Cardona, D. W. Langer, N. J. Shevchik, and J. Tejeda (unpublished)] have been reported and in both cases good agreement was found in all three lead salts between the experimentally determined valence-band density of states and those shown in Figs. 13(a)–13(c).
[33]M. Cardona, in *Optical Properties of Solids*, edited by S. Nudelman and S. S. Mitra (Plenum, New York, 1969), p. 59.

PHYSICAL REVIEW B VOLUME 8, NUMBER 4 15 AUGUST 1973

Spontaneous and Stimulated Luminescence in CdS and ZnS Excited by Multiphoton Optical Pumping

I. M. Catalano, A. Cingolani, and A. Minafra
Istituto di Fisica, Centro Studie Applicazioni in Tecnologie Avanzate, Bari, Italy
(Received 12 February 1973)

Spontaneous and stimulated emission at 85 °K in CdS and ZnS single crystals is reported. The exciting source was a ruby laser and its second harmonic. The two-photon spectrum of CdS shows stimulation effects in the phonon-assisted excitonic lines at a pumping level of about 10^{26} (photons/cm^2)/sec. The same effect is observed in cubic ZnS with the second-harmonic light. A three-photon excited spontaneous luminescence is also obtained in this last sample. The results are in good agreement with the theoretical predictions of multiphoton-absorption theory.

I. INTRODUCTION

Several authors have reported spontaneous and stimulated emission in II-VI compounds.[1–3] The mechanism responsible for most of the lasing transitions is reported[4] to involve bound excitons and acoustical-phonon-assisted transitions, particularly at very low temperatures (4.2 °K) and in the presence of impurity centers. At liquid-nitrogen temperature, line-shape measurements[1] in the spontaneous-emission spectrum have shown that in pure CdS, CdSe, and ZnO, the laser transitions involve the E_{exc}-LO line, i.e., the longitudinal optical-phonon-assisted emission of free excitons.

Other recombination mechanisms which can give laser action in II-VI compounds are the exciton-exciton[2] interaction and the excitonic-molecule recombination.[5] This last effect is difficult to observe experimentally owing to the small binding energy of the excitonic molecule, while the first one may become prominent at very low temperatures. Generally, the laser emission has been obtained by electron-beam pumping,[1,2] by linear optical pumping with ultraviolet laser light,[6] and by two-photon excitation with a ruby laser.[7]

In the present work we report stimulated emission in pure CdS and ZnS samples at a temperature of 85 °K under two-photon optical pumping, and three-photon excited spontaneous luminescence in ZnS at the same temperature.

II. BASIC THEORY

The fundamental energy gap E_g of CdS and ZnS (cubic) are, at 77 °K, 2.5 and 3.8 eV; the photon energy of the ruby laser is $\hbar\omega_1 = 1.78$ eV and that of its second harmonic is $\hbar\omega_2 = 3.56$ eV.

The nonlinear cross section γ_n for an n-photon process is defined by

$$W^{(n)} = N\gamma_n I^n , \quad (1)$$